PROCEEDINGS OF SPIE

SPIEDigitalLibrary.org/conference-proceedings-of-spie

Plasma plume expansion dynamics in nanosecond Nd:YAG laserosteotome

Hamed Abbasi, Georg Rauter, Raphael Guzman, Philippe C. Cattin, Azhar Zam

Hamed Abbasi, Georg Rauter, Raphael Guzman, Philippe C. Cattin, Azhar Zam, "Plasma plume expansion dynamics in nanosecond Nd:YAG laserosteotome," Proc. SPIE 10505, High-Speed Biomedical Imaging and Spectroscopy III: Toward Big Data Instrumentation and Management, 1050513 (20 February 2018); doi: 10.1117/12.2290980

SPIE.

Event: SPIE BiOS, 2018, San Francisco, California, United States

Plasma plume expansion dynamics in nanosecond Nd:YAG laserosteotome

Hamed Abbasi[*a], Georg Rauter[b], Raphael Guzman[c], Philippe C. Cattin[d], Azhar Zam[†a]

[a] Biomedical Laser and Optics Group, Department of Biomedical Engineering, University of Basel, Gewerbestrasse 14, CH-4123 Allschwil, Switzerland
[b] Bio-Inspired RObots for Medicine-Lab., Department of Biomedical Engineering, University of Basel, Gewerbestrasse 14, CH-4123 Allschwil, Switzerland
[c] Department of Neurosurgery, University Hospital Basel, Spitalstrasse 21, CH-4056 Basel, Switzerland
[d] Center for medical Image Analysis and Navigation, Department of Biomedical Engineering, University of Basel, Gewerbestrasse 14, CH-4123 Allschwil, Switzerland

ABSTRACT

In minimal invasive laser osteotomy precise information about the ablation process can be obtained with LIBS in order to avoid carbonization, or cutting of wrong types of tissue. Therefore, the collecting fiber for LIBS needs to be optimally placed in narrow cavities in the endoscope. To determine this optimal placement, the plasma plume expansion dynamics in ablation of bone tissue by the second harmonic of a nanosecond Nd:YAG laser at 532 nm has been studied. The laser-induced plasma plume was monitored in different time delays, from one nanosecond up to one hundred microseconds. Measurements were performed using high-speed gated illumination imaging. The expansion features were studied using illumination of the overall visible emission by using a gated intensified charged coupled device (ICCD). The camera was capable of having a minimum gate width (Optical FWHM) of 3 ns and the timing resolution (minimum temporal shift of the gate) of 10 ps. The imaging data were used to generate position–time data of the luminous plasma-front. Moreover, the velocity of the plasma plume expansion was studied based on the time-resolved intensity data. By knowing the plasma plume profile over time, the optimum position (axial distance from the laser spot) of the collecting fiber and optimal time delay (to have the best signal to noise ratio) in spatial-resolved and time-resolved laser-induced breakdown spectroscopy (LIBS) can be determined. Additionally, the function of plasma plume expansion could be used to study the shock wave of the plasma plume.

Keywords: Fast photography, time-resolved, plasma plume, laserosteotome

1. INTRODUCTION

LIBS feedback systems for laserosteotomy could help surgeons avoid cutting a wrong tissue or make it carbonized [1-9]. Laserosteotomes connected to such a feedback system are so-called smart laserosteotomes [10]. Although compared to traditional mechanical tools for cutting bones, laserosteotomes already have several benefits including minimal invasiveness, non-contact interaction, functional cuts and accelerated healing [11-15], making them smart can further improve the level of safety of the current systems [16]. In minimally invasive interventions there is little space, so the placement of the fiber with respect to an observable laser plume is critical [17-20]. This study aims to determine the optimal placement of the fiber with respect to a plasma that is easily accessible due to an ablation process carried out in open air. While most of the similar previous research has carried out to observe the expansion dynamics of the plasma from the side view (perpendicular to the laser beam) [21-23], this study aims to observe the plasma profile from frontal view. The reason for selecting the front view is the fact that in endoscopic laserosteotomy, observing the plasma zone from the side view needs much more optical components and as a result makes the endoscopes thicker. The expansion

[*] hamed.abbasi@unibas.ch; phone +41 (0)61 207 54 61; http://dbe.unibas.ch/blog

[†] azhar.zam@unibas.ch; phone +41 (0)61 207 54 60; http://dbe.unibas.ch/blog

High-Speed Biomedical Imaging and Spectroscopy III: Toward Big Data Instrumentation and Management, edited by Kevin K. Tsia, Keisuke Goda, Proc. of SPIE Vol. 10505, 1050513 · © 2018 SPIE
CCC code: 1605-7422/18/$18 · doi: 10.1117/12.2290980

behavior of the laser-driven plasma plume involves several processes such as shielding effects, electron-ion recombination, attenuation, and shock wave formation. Thus, the plasma behavior depends on laser parameters and environmental conditions including the type of sample that is ablated by the laser [24-26]. Therefore, the plasma expansion dynamic for different samples should be studied individually in order to determine the appropriate time delay and appropriate position of the collecting fiber (optimal signal to noise ratio) in time-resolved and spatial-resolved LIBS feedback systems. In this study, the emission intensities of plasma for the axial area (FWHM) as a function of delay were measured by means of high-speed gated illumination imaging with a nanosecond gated ICCD during nanosecond Nd:YAG bone ablation to find out the best possible time delay and axial distance of collection optic in smart laserosteotomes.

2. MATERIALS AND METHODS

2.1 Bone samples

In this study, fresh femur porcine bones were used. The bones were kept in the deep freezer (-18° centigrade) between the scarification to the starting day of the experiment. Four hours before the experiment, the bones were moved to the refrigerator (+ 4° centigrade). The experiments were done at room temperature after removing the surrounding soft tissue with a surgical scalpel.

2.2 Optical setup

Figure 1 shows the schematic of the experimental setup. A Q-switched Nd:YAG laser (Q-smart 450, Quantel) running in its second harmonic at 532 nm with 5 ns pulse duration was used to generate plasma in the air and at the surface of the bone. The laser was operated at 200 mJ per pulse and 1 Hz repetition rate. The first harmonic of the laser was separated and blocked using a nonlinear crystal (C), and a beam blocker (D) installed right after the harmonic generator, respectively. The initial output beam of the laser (E) (6.5 mm diameter, < 0.5 mrad divergence) was horizontally directed to a dichroic mirror (G) placed at 45 degree to the laser line. The reflected light was directed to the surface of the sample from the side by placing a convex lens (H) between the dichroic mirror and the sample (I). This focusing lens provides a spot size in the order of a couple of hundreds of micrometers at the sample surface. The image of the generated plasma (J) was passed through the mentioned convex lens and dichroic mirror first and was focused by an imaging lens (M) to the ICCD (N) (PI-MAX4, Princeton Instruments) after filtering through a laser line filter (L) (532 nm blocker). Both focusing and collimating lenses had a focal length of +40 mm for providing magnification of 1 to have an appropriate field of view. The ICCD was synchronized with the Q-switch of the laser through the internal delay generator of the ICCD to apply a desired time delay (Q-switch as a master and the camera as a slave). Although the camera had the ability of time delay adjustment with picosecond resolution, due to having 1 ns jitter of Q-switch TTL pulse output, different time delays ranging from 1 nanosecond to 100 microseconds were set. The gain and the gate of the ICCD were set to fill 90% of the available counts of the camera (16-bit digitization) to avoid non-linearity effects which normally happen near the saturation.

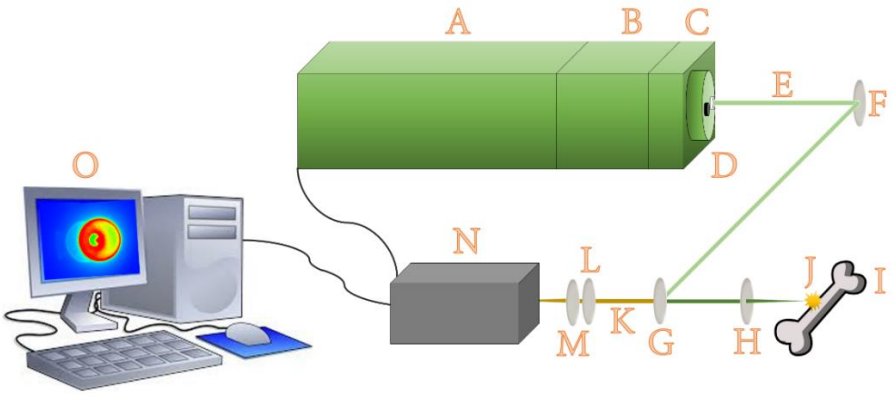

Figure 1. The schematics of the optical setup for investigating ionization front. A: Laser (pulsed Nd:YAG), B: Second harmonic generator, C: Harmonic separator, D: First harmonic blocker, E: Laser beam, F: Laser line mirror, G: Dichroic mirror, H: Convex lens, I: Sample, J: Generated plasma, K: Plasma emission light, L: Notch filter, M: Convex lens, N: ICCD, O: Computer.

3. RESULTS

3.1 Imaging of the generated plasma in air

Figure 1 shows the images of the generated plasmas in the air with different time delays ranging from 1 ns to 10 μs. The time delay shown in the top-left corner of the pictures is the time between starting point of the generation of the plasma and opening the gate of the ICCD. Imaging at each time delay was repeated five times, and the images were found to be reproducible in both shape and size. Rapid expansion is observable in the first tens of nanoseconds after the generation of the plasma, and afterwards, the plasma size was roughly constant. Table 1 shows the average size of the generated plasma in the air in millimeters, including standard deviation of five different measurements at each time delay.

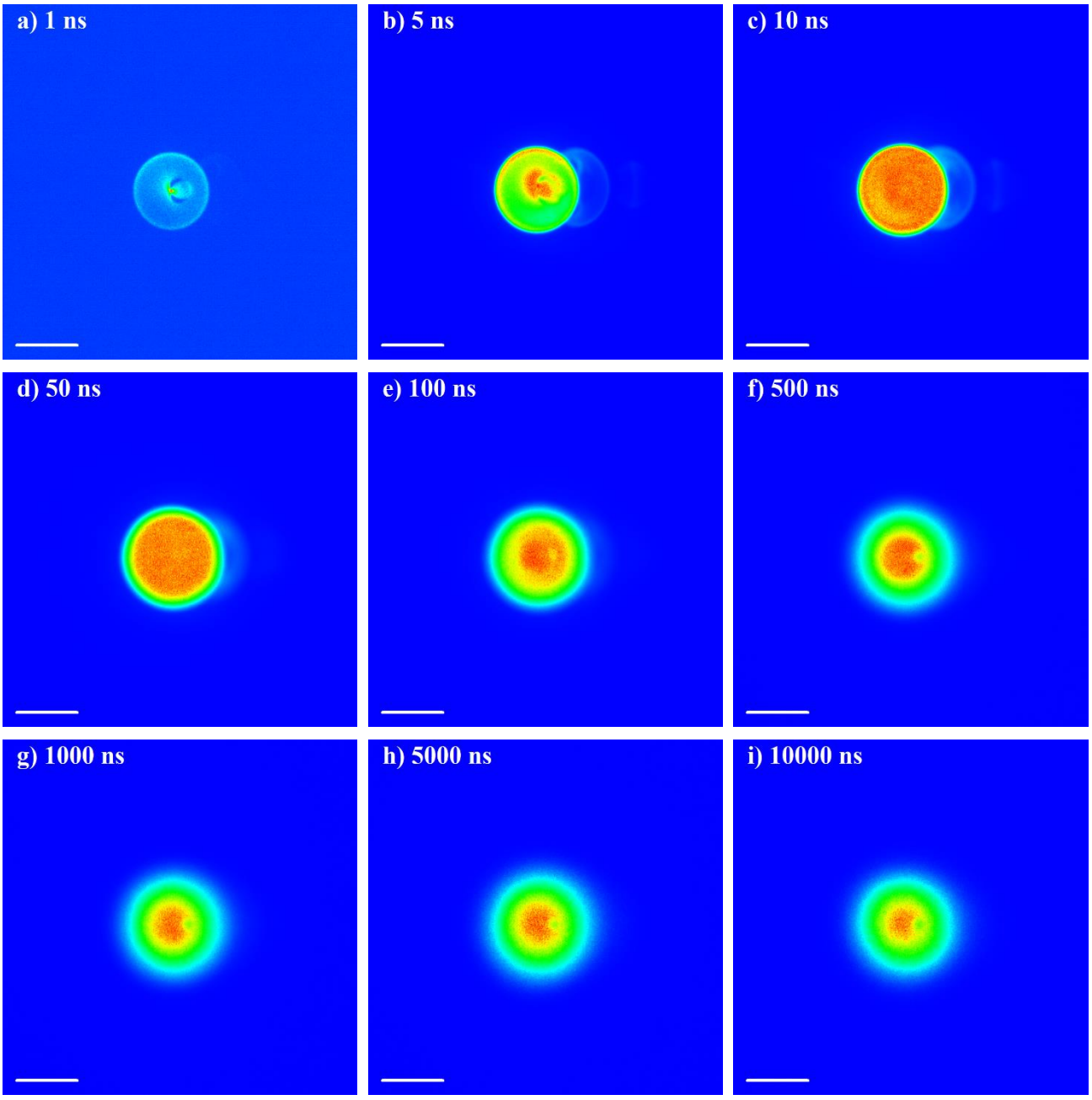

Figure 2. Images of the generated plasma in the air with different time delay. The scale bar at the corner is 2 mm in all images. Images are depicted in full-scale auto-contrast mode (Blue: minimum intensity, Red: maximum intensity).

3.2 Imaging of the generated plasma at the surface of the bone

Figure 2 shows the images of the plasma generated at the surface of the bone with different time delays ranging from 1 ns to 10 μs. The time delay shown in the top-left corner of the pictures is the time between starting point of the generation of the plasma and opening the gate of the ICCD. Imaging at each time delay was repeated five times, and similar to the measurements above, the images were found to be reproducible in both shape and size. The generated plasmas at the surface of the bone were bigger and brighter in comparison to the plasma generated in the air. High velocity expansion was observed in the first tens of nanoseconds after the generation of the plasma and later a slower expansion was observed. Table 1 shows the average size of the generated plasma at the surface of the bone in millimeter, including standard deviation of five different measurements at each time delay.

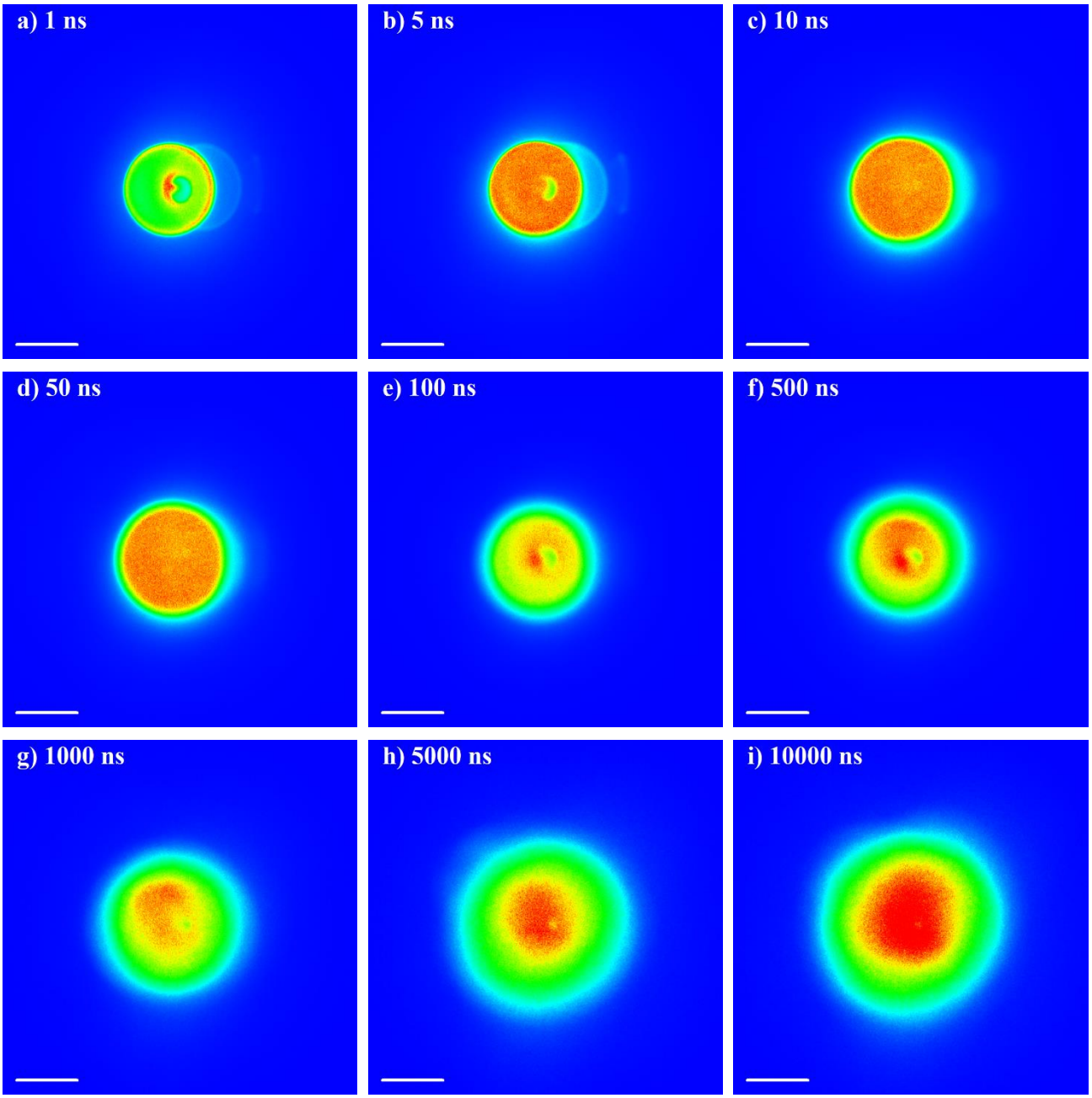

Figure 3. Images of the generated plasma at the surface of the bone with different time delay. The scale bar at the corner is 2 mm in all images. Images are depicted in full-scale auto-contrast mode (Blue: minimum intensity, Red: maximum intensity).

Table 1. The average size (FWHM) of the generated plasmas in the air and at the surface of the bone.

Time delay [ns]	Size of the plasma generated in the air [mm]	Size of the plasma generated at the surface of the bone [mm]
1	2.32± 0.04	2.88± 0.04
5	2.67± 0.04	3.07± 0.01
10	2.87± 0.01	3.38± 0.02
50	2.96± 0.01	3.64± 0.02
100	2.56± 0.02	3.07± 0.01
500	2.24± 0.02	3.17± 0.06
1000	2.19± 0.03	3.69± 0.02
5000	2.23± 0.05	3.99± 0.07
10000	2.13± 0.07	4.42± 0.17

3.3 Plasma fading

It was observed that plasma exists for tens of microseconds and then it gradually fades. It is worth mentioning that the fading happened in the air earlier than the bone. Figure 4 shows a typical plasma image of the bone sample, right before fading (100 μs delay). As can be seen from the image, the central part fades earlier than outer part, since the ionized particles in the central part of the plasma have a higher lifetime as compare to those in the outer parts.

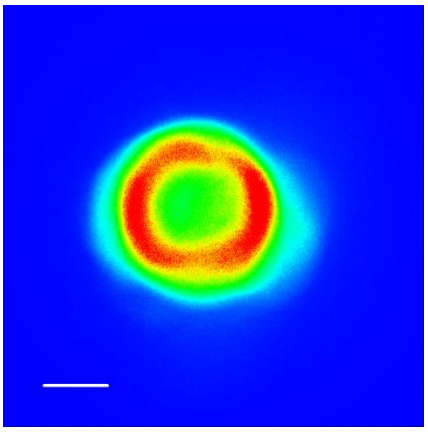

Figure 4. A typical image of the generated plasma at the surface of the bone right before fading. The scale bar at the corner is 2 mm. The image is depicted in optimal-scale auto-contrast mode (Blue: minimum intensity, Red maximum intensity).

4. DISCUSSION

It was observed that the size of the plasma generated at the surface of the bone was bigger and brighter in comparison to the plasma generated in the air in all time delays. This could be related to the fact that more particles could be ionized in the bone sample, whereas in air there are not so many particles that effectively can be ionized. Additionally, a rapid expansion with very high velocity was observed in the first tens of nanoseconds after the generation of the plasma in both samples, confirming a high level of Bremsstrahlung emission in this timescale. Therefore, a time delay of more than hundreds of nanoseconds is necessary to prevent covering the atomic plasma lines by the continuum emission in time-resolved laser-induced breakdown spectroscopy (TRLIBS) of bone samples. In the beginning of the plasma generation in

the bone, the size of plasma is less than 3.66 mm. Based on this result, if the collection fiber is placed 1.83 mm away from the center of the plasma, it would collect a high level of Bremsstrahlung-free emissions in spatial-resolved laser-induced breakdown spectroscopy (SRLIBS). However, the idea needs to be confirmed experimentally in the future. Moreover, it was observed that the plasma exists up to some hundreds of microseconds in bone samples. This observation indicates that using the laser with a repetition rate of more than 10 kHz could result in plasma shielding effects and consequently reduce the ablation efficiency due to the absorption of the laser light by the plasma itself. In addition, having different sizes and fading times between bone and air samples shows the potential of high-speed gated illumination imaging of plasma for auto-focus applications which results in having thinner cuts and more reproducible LIBS spectra for smart laserosteotomes. Finally, it should be noted that all of the experiments in this study were done with a fixed energy, pulse duration, and wavelength. Thus, the effect of changing the mentioned parameter on the results should be examined in future to optimally place the collecting fiber in narrow cavities in the endoscope of smart laserosteotomes for in vivo experiments.

5. CONCLUSION

The dynamics of the plasma plume is essential to determine the appropriate position of the collecting fiber (to have the best signal to noise ratio) in LIBS feedback systems of laserosteotomes. The emission intensities of plasma for an axial view (FWHM) as a function of delay were measured by means of high-speed gated illumination imaging with a nanosecond gated ICCD during porcine femur bone ablation with a nanosecond Nd:YAG laserosteotome. Results of the expansion dynamic of the generated plasma at the surface of the bone suggest to either have a time delay of more than hundreds of nanoseconds in TRLIBS or to put the collecting fiber ca. 1.83 mm away from the central part of the ablation zone in SRLIBS to have the best signal to noise ratio. Moreover, the results of the fading time study, which was longer in bone samples as compared to the air, suggest using lasers with a repetition rate of 10 kHz or less to avoid plasma shielding effects for nanoseconds Nd:YAG laserosteotomy.

ACKNOWLEDGMENTS

The authors gratefully acknowledge funding of the Werner Siemens Foundation through the MIRACLE (short for Minimally Invasive Robot-Assisted Computer-guided LaserosteotomE) project. Moreover, the authors are particularly appreciative of the assistance given by Ms. Lina Beltrán.

REFERENCES

[1] Mehari, F., Rohde, M., Knipfer, C., Kanawade, R., Klämpfl, F., Adler, W., Stelzle, F. and Schmidt, M., "Laser induced breakdown spectroscopy for bone and cartilage differentiation-ex vivo study as a prospect for a laser surgery feedback mechanism," Biomedical optics express, 5(11), pp.4013-4023 (2014).

[2] Mehari, F., Rohde, M., Kanawade, R., Knipfer, C., Adler, W., Klämpfl, F., Stelzle, F. and Schmidt, M., "Investigation of the differentiation of ex vivo nerve and fat tissues using laser-induced breakdown spectroscopy (LIBS): Prospects for tissue-specific laser surgery," Journal of biophotonics, 9(10), pp.1021-1032 (2016).

[3] Henn, K., Gubaidullin, G.G., Bongartz, J., Wahrburg, J., Roth, H. and Kunkel, M., "A spectroscopic approach to monitor the cut processing in pulsed laser osteotomy," Lasers in medical science, 28(1), pp.87-92 (2013).

[4] Ferraz de Menezes, R., Harvey, C.M., Márquez de Martínez Gerbi, M.E., Smith, Z.J., Smith, D., Ivaldi, J.C., Phillips, A., Chan, J.W. and Wachsmann-Hogiu, S., "Fs-laser ablation of teeth is temperature limited and provides information about the ablated components," Journal of Biophotonics, 10(10), pp. 1292-1304 (2017).

[5] Han, J.H., Moon, Y., Lee, J.J., Choi, S., Kim, Y.C. and Jeong, S., "Differentiation of cutaneous melanoma from surrounding skin using laser-induced breakdown spectroscopy," Biomedical optics express, 7(1), pp.57-66 (2016).

[6] Yueh, F.Y., Zheng, H., Singh, J.P. and Burgess, S., 2009. "Preliminary evaluation of laser-induced breakdown spectroscopy for tissue classification," Spectrochimica Acta Part B: Atomic Spectroscopy, 64(10), pp.1059-1067.

[7] Jeong, D.C., Tsai, P.S. and Kleinfeld, D., "Prospect for feedback guided surgery with ultra-short pulsed laser light," Current opinion in neurobiology, 22(1), pp.24-33 (2012).
[8] Abbasi, H., Rauter, G., Guzman, R., Cattin, P.C. and Zam, A., "Laser-induced breakdown spectroscopy as a potential tool for auto carbonization detection in laserosteotomy," Submitted (2018).
[9] Nguendon, H.K., Faivre, N., Meylan, B., Shevchik, S., Rauter, G., Guzman, R., Cattin, P.C., Wasmer, K. and Zam, A. "Characterization of ablated porcine bone and muscle using laser-induced acoustic wave method for tissue differentiation," Proc. SPIE 10417, pp. 104170N1-10 (2017).
[10] Huang, H., Yang, L.M., Bai, S. and Liu, J., "Smart surgical tool," Journal of biomedical optics, 20(2), pp.028001-028001 (2015).
[11] Jowett, N., Wöllmer, W., Reimer, R., Zustin, J., Schumacher, U., Wiseman, P.W., Mlynarek, A.M., Böttcher, A., Dalchow, C.V., Lörincz, B.B. and Knecht, R., "Bone ablation without thermal or acoustic mechanical injury via a novel picosecond infrared laser (PIRL)," Otolaryngology--Head and Neck Surgery, 150(3), 385-393 (2014)
[12] Moslemi, N., Shahnaz, A., Masoumi, S., Torabi, S. and Akbari, S., "Laser-Assisted Osteotomy for Implant Site Preparation: A Literature Review," Implant dentistry, 26(1), pp.129-136 (2017).
[13] Beltrán, L., Abbasi, H., Rauter, G., Friederich, N., Cattin, P. and Zam, A., "Effect of laser pulse duration on ablation efficiency of hard bone in microseconds regime," Proc. SPIE 10453, pp. 104531S1-6 (2017).
[14] Abbasi, H., Beltrán, L., Rauter, G., Guzman, R., Cattin, P.C. and Zam, A., "Effect of cooling water on ablation in Er: YAG laserosteotome of hard bone," Proc. SPIE 10453, pp. 104531I1-4 (2017).
[15] Tulea, C.A., Caron, J., Gehlich, N., Lenenbach, A., Noll, R. and Loosen, P., "Laser cutting of bone tissue under bulk water with a pulsed ps-laser at 532 nm," Journal of biomedical optics, 20(10), 105007-105007 (2015).
[16] Abbasi, H., Rauter, G., Guzman, R., Cattin, P.C. and Zam, A., "Differentiation of femur bone from surrounding soft tissue using laser-induced breakdown spectroscopy as a feedback system for Smart Laserosteotomy," accepted to be published in Proc. SPIE (2018).
[17] Burgner, J., [Robot assisted laser osteotomy], KIT Scientific Publishing (2010).
[18] Burgner, J., Müller, M., Raczkowsky, J. and Wörn, H., "Ex vivo accuracy evaluation for robot assisted laser bone ablation," The International Journal of Medical Robotics and Computer Assisted Surgery, 6(4), pp.489-500 (2010).
[19] Sotsuka, Y., Nishimoto, S., Tsumano, T., Kawai, K., Ishise, H., Kakibuchi, M., Shimokita, R., Yamauchi, T. and Okihara, S.I., "The dawn of computer-assisted robotic osteotomy with ytterbium-doped fiber laser," Lasers in medical science, 29(3), pp.1125-1129 (2014).
[20] Stübinger, S., Landes, C., Seitz, O. and Sader, R., "Er: YAG laser osteotomy for intraoral bone grafting procedures: a case series with a fiber-optic delivery system," Journal of periodontology, 78(12), pp.2389-2394 (2007).
[21] Nahen, K. and Vogel, A., "Plume dynamics and shielding by the ablation plume during Er: YAG laser ablation," Journal of Biomedical Optics, 7(2), pp.165-178 (2002).
[22] Verhoff, B., Harilal, S.S., Freeman, J.R., Diwakar, P.K. and Hassanein, A., "Dynamics of femto-and nanosecond laser ablation plumes investigated using optical emission spectroscopy," Journal of Applied Physics, 112(9), p.093303 (2012).
[23] Camacho, J.J., Diaz, L., Marin-Roldan, A., Moncayo, S. and Caceres, J.O., "Plume Dynamics of Laser-Produced Swine Muscle Tissue Plasma," Applied spectroscopy, 70(7), pp.1228-1238 (2016).
[24] Vogel, A. and Venugopalan, V., "Mechanisms of pulsed laser ablation of biological tissues," Chemical reviews, 103(2), pp.577-644 (2003).
[25] Vogel, A., Apitz, I., Freidank, S. and Dijkink, R., "Sensitive high-resolution white-light Schlieren technique with a large dynamic range for the investigation of ablation dynamics," Optics letters, 31(12), pp.1812-1814 (2006).
[26] Nazeri, M., Majd, A.E., Massudi, R., Tavassoli, S.H., Mesbahinia, A. and Abbasi, H., "Laser-Induced Breakdown Spectroscopy Via the Spatially Resolved Technique Using Non-Gated Detector," Journal of Russian Laser Research, 37(2), pp.164-171 (2016).